1768 *Chem. Mater.* **2010,** *22,* 1768–1775
DOI:10.1021/cm903467p

CHEMISTRY OF MATERIALS
Article

# Templated Fabrication of Periodic Arrays of Metallic Attoliter Petri Dishes

Xuefeng Liu,*,† Chih-Hung Sun,‡ and Peng Jiang*,‡

†*School of Chemical and Material Engineering, Jiangnan University, Wuxi, Jiangsu 214122, China, and* ‡*Department of Chemical Engineering, University of Florida, Gainesville, Florida 32611*

*Received November 13, 2009*

Arrays of microcontainers, which allow handling and isolating a small volume of liquids, are of great technological importance in the miniaturization of analytical and bioanalytical techniques. Here we report a scalable bottom-up approach for fabricating wafer-sized, periodic arrays of metallic Petri dishes with a volume as small as 10 attoliter/dish. A monolayer, nonclose-packed colloidal crystal prepared by a spin-coating technology is first used as a structural template to create ordered microwells with vertical sidewalls. Sputtering deposition of metals on the microwells, followed by removal of template, results in the formation of isolated metallic Petri dishes. The size, separation, depth, thickness, and metal types of the resulting Petri dishes can be easily tuned by adjusting the size of the colloidal microspheres and the templating conditions. We have also demonstrated that templated gold Petri dish arrays show strong surface-enhanced Raman scattering from adsorbed benzenethiol molecules. This bottom-up technology is compatible with standard microfabrication, promising for applications ranging from biomicroanalysis to surface plasmon devices.

## Introduction

Periodic metallic nanostructures exhibit unique surface-plasmon properties that enable a broad range of important applications ranging from integrated nano-optical circuits and metamaterials to drug delivery and biosensing.[1−7] Top-down nanolithography, such as electron-beam lithography and focused ion-beam, can generate arbitrary nanostructures, but the low throughput and the high cost of these technologies are major limiting factors for large-scale production of practical devices.[8] Bottom-up colloidal self-assembly and sequential templating nanofabrication have been extensively explored as a simple and inexpensive alternative to nanolithography in creating periodic nanostructures. For instance, periodic metal nanoparticles created by nanosphere lithography (NSL), which uses a self-assembled monolayer or double-layer colloidal crystal as the sacrificial deposition mask, have been demonstrated as efficient surface-enhanced Raman scattering (SERS) substrates for sensitive chemical and biological sensing.[9−11] Angled deposition further expands the capability of NSL in fabricating more complex nanostructures (e.g., nanocrescent moons and binary metal nanoparticles).[12−16] Another aspect of NSL is to use the spontaneously organized colloidal arrays as an etching mask to transfer the periodic colloidal microstructure into the underneath substrate by conventional dry or wet etching.[17−19] Additionally, multilayer colloidal crystals have also been widely utilized as a sacrificial template to create three-dimensional (3-D) ordered macroporous materials that are of great technological importance in developing photonic crystals, separation membranes, and SERS substrates.[20−24]

*Corresponding author. E-mail: xfliu@jiangnan.edu.cn (X.L.), pjiang@che.ufl.edu (P.J.).

(1) Stewart, M. E.; Anderton, C. R.; Thompson, L. B.; Maria, J.; Gray, S. K.; Rogers, J. A.; Nuzzo, R. G. *Chem. Rev.* **2008**, *108*, 494.
(2) Ozbay, E. *Science* **2006**, *311*, 189.
(3) Barnes, W. L.; Dereux, A.; Ebbesen, T. W. *Nature* **2003**, *424*, 824.
(4) Murray, W. A.; Barnes, W. L. *Adv. Mater.* **2007**, *19*, 3771.
(5) Camden, J. P.; Dieringer, J. A.; Zhao, J.; Van Duyne, R. P. *Acc. Chem. Res.* **2008**, *41*, 1653.
(6) Wang, H.; Brandl, D. W.; Nordlander, P.; Halas, N. J. *Acc. Chem. Res.* **2007**, *40*, 53.
(7) Henzie, J.; Lee, M. H.; Odom, T. W. *Nat. Nanotech.* **2007**, *2*, 549.
(8) Levene, M. J.; Korlach, J.; Turner, S. W.; Foquet, M.; Craighead, H. G.; Webb, W. W. *Science* **2003**, *299*, 682.
(9) Haynes, C. L.; Van Duyne, R. P. *J. Phys. Chem. B* **2001**, *105*, 5599.
(10) Zhang, X. Y.; Young, M. A.; Lyandres, O.; Van Duyne, R. P. *J. Am. Chem. Soc.* **2005**, *127*, 4484.
(11) Dieringer, J. A.; McFarland, A. D.; Shah, N. C.; Stuart, D. A.; Whitney, A. V.; Yonzon, C. R.; Young, M. A.; Zhang, X. Y.; Van Duyne, R. P. *Faraday Discuss.* **2006**, *132*, 9.
(12) Gwinner, M. C.; Koroknay, E.; Fu, L. W.; Patoka, P.; Kandulski, W.; Giersig, M.; Giessen, H. *Small* **2009**, *5*, 400.
(13) Zhang, G.; Wang, D. Y. *J. Am. Chem. Soc.* **2008**, *130*, 5616.
(14) Liu, G. L.; Lu, Y.; Kim, J.; Doll, J. C.; Lee, L. P. *Adv. Mater.* **2005**, *17*, 2683.
(15) Lu, Y.; Liu, G. L.; Kim, J.; Mejia, Y. X.; Lee, L. P. *Nano Lett.* **2005**, *5*, 119.
(16) Kosiorek, A.; Kandulski, W.; Chudzinski, P.; Kempa, K.; Giersig, M. *Nano Lett.* **2004**, *4*, 1359.
(17) Jang, S. G.; Choi, D. G.; Heo, C. J.; Lee, S. Y.; Yang, S. M. *Adv. Mater.* **2008**, *20*, 4862.
(18) Choi, D. G.; Kirn, S.; Lee, E.; Yang, S. M. *J. Am. Chem. Soc.* **2005**, *127*, 1636.
(19) Choi, D. G.; Yu, H. K.; Jang, S. G.; Yang, S. M. *J. Am. Chem. Soc.* **2004**, *126*, 7019.
(20) Blanco, A.; Chomski, E.; Grabtchak, S.; Ibisate, M.; John, S.; Leonard, S. W.; Lopez, C.; Meseguer, F.; Miguez, H.; Mondia, J. P.; Ozin, G. A.; Toader, O.; van Driel, H. M. *Nature* **2000**, *405*, 437.
(21) Vlasov, Y. A.; Bo, X. Z.; Sturm, J. C.; Norris, D. J. *Nature* **2001**, *414*, 289.
(22) Rinne, S. A.; Garcia-Santamaria, F.; Braun, P. V. *Nat. Photonics* **2008**, *2*, 52.
(23) Zeng, Y.; He, M.; Harrison, D. J. *Angew. Chem., Int. Ed.* **2008**, *47*, 6388.
(24) Tessier, P. M.; Velev, O. D.; Kalambur, A. T.; Rabolt, J. F.; Lenhoff, A. M.; Kaler, E. W. *J. Am. Chem. Soc.* **2000**, *122*, 9554.


Published on Web 02/01/2010
© 2010 American Chemical Society

However, several drawbacks of traditional colloidal self-assemblies and templating nanofabrication have greatly impeded the practical applications of these bottom-up techniques. First, conventional colloidal crystallization techniques are tedious and incompatible with standard microfabrication, limiting throughput, and on-chip integration of practical devices. It typically takes days to make a centimeter-sized colloidal crystal.[20,25] Second, only limited, close-packed crystalline structures are available through common colloidal assemblies. Various post-treatment techniques, such as reactive ion etching (RIE), have been developed to create nonclose-packed crystals.[26] However, the spherical shape and the smooth surface of the templating colloidal spheres are not preserved during RIE. Third, deposition-based NSL is usually only appropriate for fabricating simple planar nanostructures.[9] Creating self-standing, isolated metallic nanostructures with 3-D geometries by NSL is not trivial.[27]

We have recently demonstrated a versatile spin-coating technology that enables the rapid production of wafer-sized colloidal crystals with remarkably large domain sizes and unusual nonclose-packed structures.[28,29] Spin-coating also provides a scalable templating nanofabrication platform for producing a large variety of periodic metallic nanostructures. For example, monolayer non-close-packed colloidal crystals are used as a shadow mask during electron-beam evaporation to produce periodic metallic nanohole arrays.[30] Ordered metallic nanopyramids with nanoscale sharp tips are created by using metallic nanohole arrays as second-generation template.[31] The modulated surfaces of spin-coated colloidal crystals have been demonstrated to function as a 2-D template to create metallic gratings with crystalline arrays of nanovoids.[32] Importantly, these templating techniques are compatible with standard microfabrication, allowing large-area production and patterning of complex microstructures for on-chip integration of practical devices. However, only continuous metal films with interconnecting nanostructures have been achieved so far by our previous templating approaches.

Here we report a novel spin-coating-based templating technology for fabricating isolated metallic Petri dishes with attoliter-scale volume. These microcontainers allow handling and isolating small volumes of liquids, or even single molecules, promising for the miniaturization of analytical and bioanalytical techniques.[33−35] Two distinctive characteristics of the spin-coated colloidal crystals enable the creation of isolated Petri dishes. First, in sharp contrast with colloidal crystals created by traditional self-assemblies, shear-aligned crystalline arrays are nonclose-packed.[28] This ensures the resulting Petri dishes are well separated from each other. Second, a thin and uniform polymer wetting layer separates the colloidal layer and the substrate.[36] As demonstrated later, this wetting layer determines the height of the templated Petri dishes. We have also shown that gold Petri dish arrays exhibit strong surface-enhanced Raman scattering from benzenethiol molecules adsorbed on the metal surface. Although the isolated Petri dish arrays have not been optimized, they show higher SERS enhancement factor than spin-coating-enabled continuous nanopyramid arrays.[31]

## Experimental Section

**Materials and Substrates.** All solvents and chemicals are of reagent quality and are used without further purification. Monodispersed silica spheres with ~260 nm diameter and less than 5% diameter standard deviation are synthesized by the Stöber method.[37] Ethoxylated trimethylolpropane triacrylate (ETPTA) monomer is obtained from Sartomer (Exton, PA). The photoinitiator, Darocur 1173 (2-hydroxy-2-methyl-1-phenyl-1-propanone), is provided by Ciba Specialty Chemicals. (3-Acryloxypropyl)trichlorosilane (APTCS) is purchased from Gelest. Silicon wafers [test grade, n type, (100)] are obtained from Wafernet and are primed by swabbing APTCS on the wafer surface using cleanroom Q-tips (Fisher), rinsed and wiped with 200-proof ethanol three times, spin coated with a 200-proof ethanol rinse at 3000 rpm for 1 min, and baked on a hot plate at 110 °C for 2 min. CR-7 chromium etchant is obtained from Transene. Benzenethiol (>98% purity) is purchased from Sigma-Aldrich.

**Instrumentation.** Scanning electron microscopy (SEM) is carried out on a JEOL 6335F FEG-SEM. A WS-400B-6NPP-Lite Spin Processor (Laurell) is used to spin-coat colloidal suspensions. The photopolymerization of ETPTA monomer is carried out on a pulsed UV curing system (RC 742, Xenon). Oxygen plasma etching is performed on a Unaxis Shuttlelock RIE/ICP reactive-ion etcher. A Kurt J. Lesker CMS-18 multitarget sputter is used to deposit metals. Raman spectra are measured with a Renishaw inVia confocal Raman microscope.

**Templated Preparation of Gold Petri Dish Arrays.** The fabrication of a wafer-scale, monolayer, nonclose-packed silica colloidal crystal-polymer nanocomposite is performed according to the established spin-coating procedures.[28,29] In short, Stöber silica colloids are first dispersed in ETPTA monomer (with 2 wt % Darocur 1173 photoinitiator) to make a final particle volume fraction of 20%. The colloidal suspension is disposed on an APTCS-primed silicon wafer and spin-coated at 200 rpm for 120 s, 300 rpm for 120 s, 1000 rpm for 60 s, 3000 rpm for 20 s, 6000 rpm for 20 s, and finally 8000 rpm for 360 s. ETPTA monomer is rapidly polymerized for 4 s by using a pulsed UV curing system. The polymer matrix is partially

(25) Jiang, P.; Bertone, J. F.; Hwang, K. S.; Colvin, V. L. *Chem. Mater.* **1999**, *11*, 2132.
(26) Deng, T.; Cournoyer, J. R.; Schermerhorn, J. H.; Balch, J.; Du, Y.; Blohm, M. L. *J. Am. Chem. Soc.* **2008**, *130*, 14396.
(27) Heo, C. J.; Kim, S. H.; Jang, S. G.; Lee, S. Y.; Yang, S. M. *Adv. Mater.* **2009**, *21*, 1726.
(28) Jiang, P.; McFarland, M. J. *J. Am. Chem. Soc.* **2004**, *126*, 13778.
(29) Jiang, P.; Prasad, T.; McFarland, M. J.; Colvin, V. L. *Appl. Phys. Lett.* **2006**, *89*, 011908.
(30) Jiang, P.; McFarland, M. J. *J. Am. Chem. Soc.* **2005**, *127*, 3710.
(31) Sun, C. H.; Linn, N. C.; Jiang, P. *Chem. Mater.* **2007**, *19*, 4551.
(32) Jiang, P. *Angew. Chem., Int. Ed.* **2004**, *43*, 5625.
(33) Chiu, D. T.; Wilson, C. F.; Ryttsen, F.; Stromberg, A.; Farre, C.; Karlsson, A.; Nordholm, S.; Gaggar, A.; Modi, B. P.; Moscho, A.; Garza-Lopez, R. A.; Orwar, O.; Zare, R. N. *Science* **1999**, *283*, 1892.
(34) Grzybowski, B. A.; Haag, R.; Bowden, N.; Whitesides, G. M. *Anal. Chem.* **1998**, *70*, 4645.
(35) Jackman, R. J.; Duffy, D. C.; Ostuni, E.; Willmore, N. D.; Whitesides, G. M. *Anal. Chem.* **1998**, *70*, 2280.
(36) Sun, C. H.; Min, W. L.; Jiang, P. *Chem. Commun.* **2008**, 3163.
(37) Stöber, W.; Fink, A.; Bohn, E. *J. Colloid Interface Sci.* **1968**, *26*, 62.

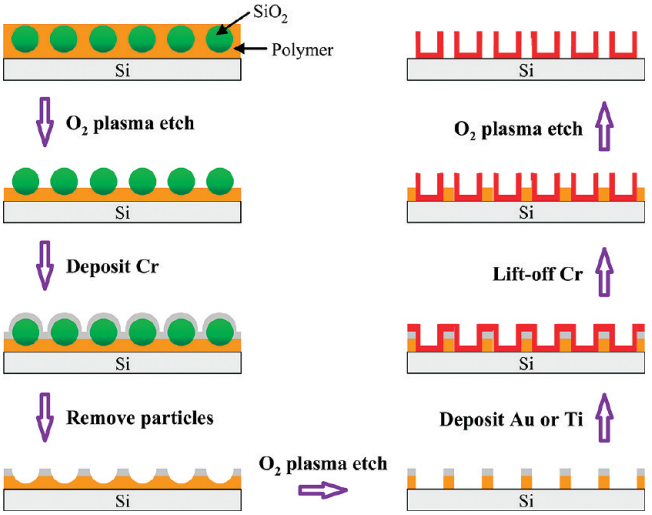


**Figure 1.** Schematic outline of the templating procedures for fabricating periodic arrays of metallic Petri dishes by using spin-coated silica colloidal crystal as template.

removed by using a reactive ion etcher operating at 40 mTorr oxygen pressure, 40 SCCM flow rate, and 100 W for 70 s. A 50 nm layer of Cr is deposited on the sample using a sputtering deposition at a typical deposition rate of 1.6 Å/s. The wafer is then rinsed in deionized water and rubbed with a cleanroom Q-tip to remove Cr-coated silica spheres. Another oxygen plasma etching is performed at the above conditions for 195 s, followed by sputtering-deposition of a 50 nm layer of Ti or Au. The sacrificial Cr layer is lifted-off by dissolving in a CR-7 chromium etchant for 20 s. Finally, the remaining ETPTA polymer between the templated metallic Petri dishes is removed by oxygen plasma etching operating at the above conditions for 195 s.

**Raman Spectra Measurement.** The silicon wafer with the templated Au Petri dishes is immersed in a 5 mM solution of benzenethiol in 200-proof ethanol for 40 min and then rinsed in 200-proof ethanol for several minutes. The samples are allowed to dry in air for 20 min, after which the Raman spectra are measured. A flat Au film deposited on a glass microslide using the same sputtering process is utilized as the control sample for Raman spectra measurement. Raman spectra are obtained using a 50× objective with a 40 $\mu m^2$ spot size and a 785 nm diode laser at 2.5 mW with integration time of 10 s.

## Results and Discussion

The schematic outline of the templating procedures for fabricating periodic arrays of metallic Petri dishes by using spin-coated silica colloidal crystal as template is shown in Figure 1. The spin-coating technology is based on shear-aligning uniform colloids suspended in a nonvolatile monomer (ETPTA) by using standard spin-coating equipment.[28,29] Silica spheres with diameter ranging from tens of nanometers to several micrometers have been successfully organized over wafer-sized (up to 8-in.) areas by this scalable and microfabrication-compatible bottom-up approach.[28,38] The thickness of the resulting colloidal crystals can be easily tuned from a monolayer to hundreds of layers by adjusting the spin-coating conditions.[28] Here we utilize spin-coated monolayer crystals as template.

(38) Min, W. L.; Jiang, P.; Jiang, B. *Nanotechnology* **2008**, *19*, 475604.

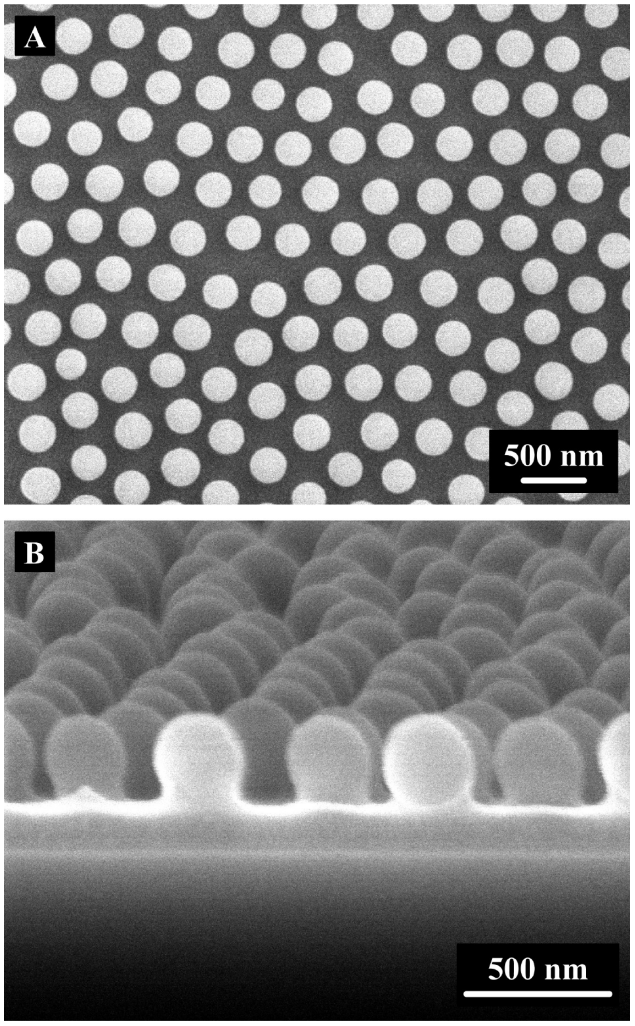


**Figure 2.** (A) Top- and (B) side-view SEM images of a partially embedded silica colloidal crystal consisting of 265 nm spheres in ETPTA polymer prepared by spin-coating and sequential oxygen plasma etching.

We first perform oxygen plasma etching to selectively remove the ETPTA polymer matrix for partially releasing the embedded silica arrays. A thin layer of Cr is then deposited by sputtering, covering the surface of the released silica spheres and the exposed ETPTA polymer. After removing the loosely attached silica spheres by scrubbing using a cleanroom Q-tip under flowing water, hemisphere-shaped polymer vials separated by arrays of Cr nanoholes are formed. The Cr layer protects the underneath polymer from being etched during a second oxygen plasma etching process, while the unprotected polymer layer is etched down to the substrate to form vertical microwells. A thin layer of Ti or Au is then uniformly deposited on the top and sidewall of the microwells by isotropic sputtering. After lifting-off Cr by wet etching and removing residual polymer by oxygen plasma etching, periodic arrays of metallic Petri dishes are resulted.

Figure 2 shows top- and side-view scanning electron microscopy (SEM) images of a spin-coated monolayer colloidal crystal consisting of silica spheres with 265 ± 8 nm diameter. The ETPTA polymer matrix surrounding the silica colloids has been partially removed by oxygen plasma etching to release the embedded particles.

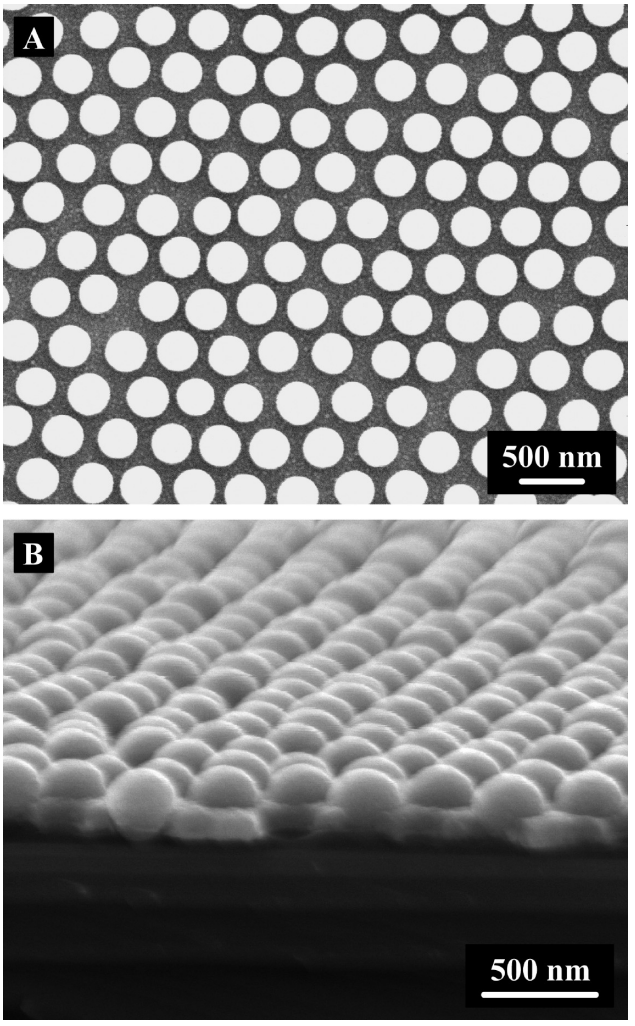


**Figure 3.** (A) Top- and (B) side-view SEM images of a colloidal monolayer sample as in Figure 2 coated with a 50 nm layer of Cr.

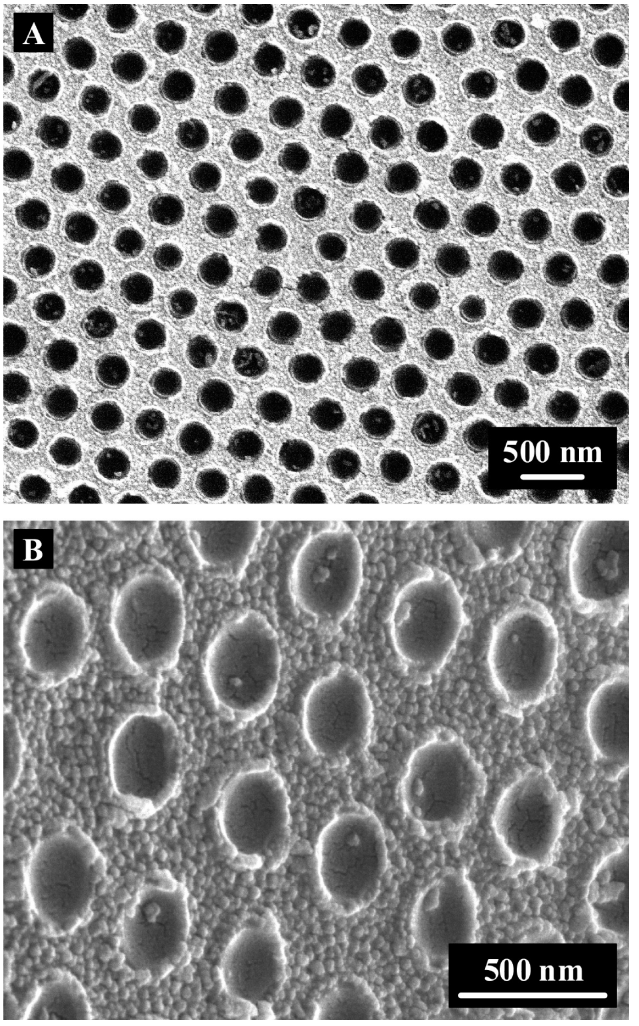


**Figure 4.** (A) Top- and (B) tilted-view (45°) SEM images of a Cr nanohole array on polymer microvials prepared by removing silica spheres from a metallized monolayer sample as shown in Figure 3.

The nonclose-packing of the shear-aligned colloidal array is clearly evident. The interparticle distance between neighboring colloids is determined to be ~1.4-times of the diameter of silica spheres by pair correlation function (PCF) calculation.[29] The colloidal array shows only short-range ordering as the images are taken from polycrystalline regions that separate single-crystalline domains which are typically several hundred micrometers in size.[29] From the side-view SEM image in Figure 2B, the uniform polymer wetting layer (~150 nm thick) that separates the colloidal layer and the substrate is apparent. As demonstrated later, the thickness of this wetting layer determines the height of the templated Petri dishes. Preliminary results show that thicker wetting layer (i.e., taller Petri dishes) can be obtained by shear-aligning nonclose-packed colloidal monolayer on an ETPTA layer which has been coated on the substrate prior to spin-coating.

A thin sacrificial layer of Cr is then deposited on the sample surface by sputtering. Besides Cr, many other materials, such as Al and silicon oxide, can also be used as the sacrificial layer. Figure 3 shows SEM images of a colloidal monolayer coated with 50 nm thick Cr. From the top-view SEM image in Figure 3A, it is clear that the metal-coated silica particles retain the spherical shape, while the particle size (302 ± 7 nm) is larger than that of the bare silica spheres as shown in Figure 2A. The conformal deposition of Cr on both surfaces of silica colloids and ETPTA polymer is confirmed by the side-view SEM image as shown in Figure 3B. The silica particles are only loosely attached to the substrate, and a gentle rub using a cleanroom Q-tip under flowing water is sufficient to remove all templating particles without affecting the remaining metal coating and the polymer wetting layer.[30] This results in the formation of periodic Cr nanoholes on polymer microvial arrays as shown by the top- and tilted-view SEM images in Figure 4 (parts A and B, respectively). The aligned nanoholes and microvials are both templated from spin-coated silica spheres. The average diameter of the resulting microvials is determined to be 204 ± 5 nm, which is smaller than the size of the templating silica spheres. From Figure 4B, it is apparent that the residual polymer microvials are shallow, indicating only the bottom part of the templating silica spheres is replicated to create smaller microvials.

The ordered Cr nanoholes can be used as a second-generation etching mask during an oxygen plasma etching

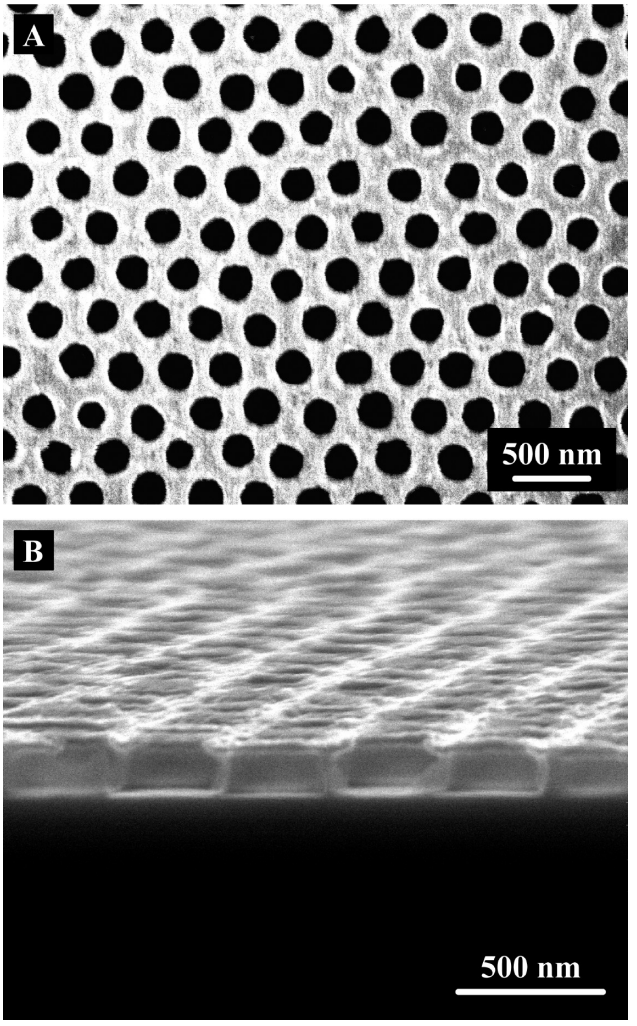


**Figure 5.** (A) Top- and (B) side-view SEM images of an array of microwells with vertical sidewalls prepared by brief oxygen plasma etching of the nanohole array sample as shown in Figure 4.

process. The unprotected ETPTA polymer is etched faster than the polymer underneath Cr, resulting in the formation of polymer microwells with vertical sidewalls. Prolonged plasma etching leads to undercut of the polymer wetting layer beneath Cr nanoholes. By adjusting the dry etching duration, the amount of undercut and the thickness of the sidewalls that separate adjacent microwells can be precisely controlled. Figure 5 shows SEM images of a nanohole array sample prepared by 195 s oxygen plasma etching of the sample in Figure 4. By comparing the SEM images in Figures 4 and 5A, it is evident that the diameter of the Cr nanoholes is preserved during the oxygen plasma etching process. The diameter of the polymer microwells is estimated from the cross-sectional SEM image in Figure 5B to be ~370 nm, larger than that of the original silica spheres. This clearly demonstrates the undercutting of the polymer layer underneath Cr.

Sputtering is then applied to deposit a thin layer of metal on the templated microwell arrays. As sputtering

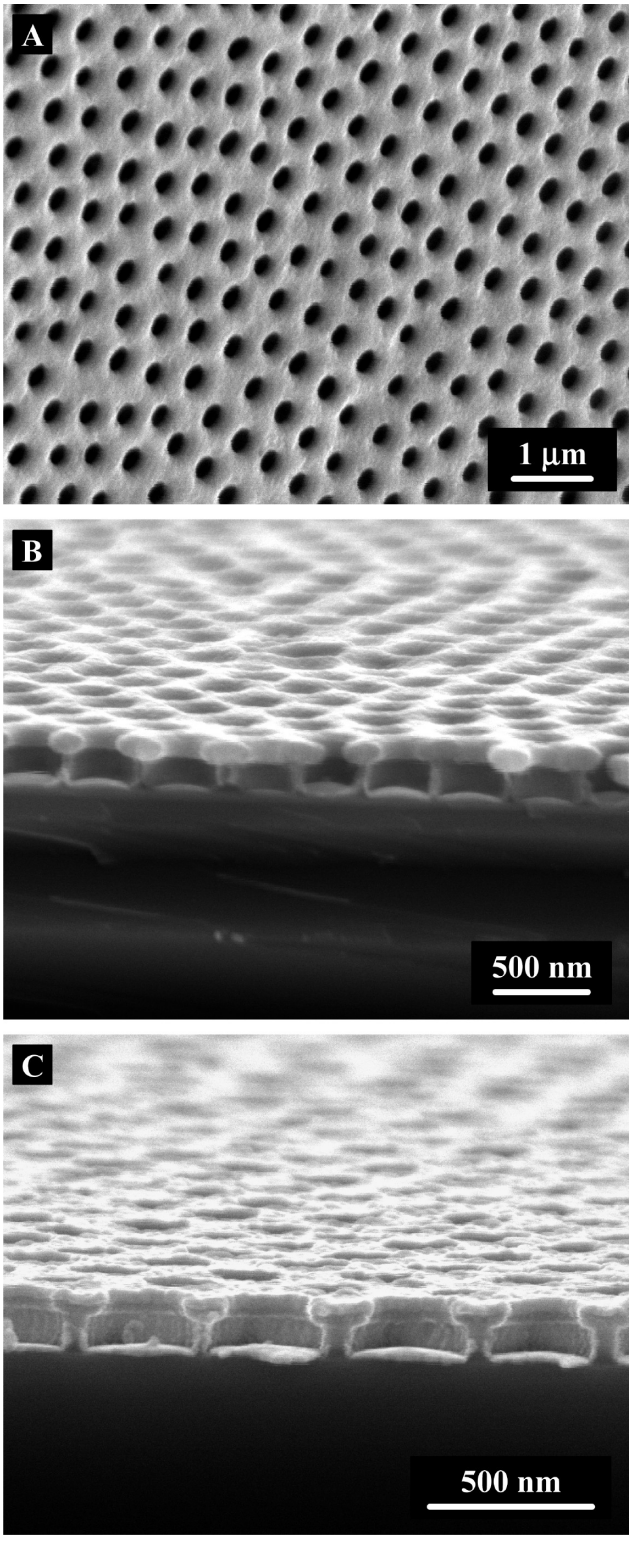


**Figure 6.** SEM images of an array of microwells coated with a thin layer of metal by sputtering. (A) Tilted (45°) view of a sample coated with 50 nm Ti. (B) Cross-sectional view of the same sample as in (A). (C) Cross-sectional view of a sample coated with 50 nm Au.

deposition is an isotropic process,[39] a uniform coating is formed on the surfaces of the Cr nanoholes, the exposed substrate, and the sidewalls of the microwells. Figure 6A, B shows tilted (45°) and cross-sectional SEM images of a microwell sample coated with 50 nm thick Ti. The opening of the nanoholes (161 ± 10 nm) is apparently smaller

(39) Madou, M. J. *Fundamentals of Microfabrication: the Science of Miniaturization*, 2nd ed.; CRC Press: Boca Raton, FL, 2002.

than that of the Cr nanohole array sample as shown in Figure 5A (212 ± 10 nm). The conformal deposition of the sputtered metal on the polymer sidewalls is demonstrated by the cross-sectional images in Figure 6B,C, which show microwells coated with 50 nm thick Ti and Au, respectively. We have also tested consecutive sputtering deposition of multiple metals (e.g., Au−Ag−Au) and metal−insulator (such as Au−$SiO_2$−Au) in a well-controlled manner. Similar conformal deposition as the above single-metal case is observed, and composite Petri dishes with multilayer structure are the result.

The sacrificial Cr layer can then be dissolved in a CR-7 etchant to lift-off metal deposited above it. Figure 7 shows top- and side-view SEM images of the same sample as shown in Figure 6C after the lift-off process. As Au has higher electron density than polymer, it appears brighter in the SEM images. This leads to the ringlike structure as shown in Figure 7A. The average diameter of the metal Petri dishes is determined to be 317 ± 11 nm. The bottom of the metallic Petri dishes can be clearly seen from the side-view SEM image in Figure 7B. The thickness of the bottom metal is almost identical to that of the sidewalls, indicating conformal deposition of material during the sputtering process. Debris is found in many Petri dishes as shown in Figure 7A,B. The Energy Dispersive X-ray (EDX) spot-analysis shows the debris is residual Au dust that is generated by ultrasonication in the above lift-off process. By briefly ultrasonicating the contaminated sample in a second water bath, most debris can be removed (see the Ti Petri dishes in Figure 8C after a 2-min ultrasonication treatment).

The residual polymer between metallic Petri dishes can finally be removed by oxygen plasma etching, leaving behind periodic arrays of metallic Petri dishes. Figure 8A shows a photograph of a 4-in.-sized Au Petri dish sample illuminated with white light. The iridescent colors come from the angle-dependent Bragg diffraction of visible light by the periodic array of metal dishes which is confirmed by the top-view SEM image as shown in Figure 8B. The same templating approach can be easily extended to other materials to create periodic Petri dishes. Figure 8C,D shows top- and side-view SEM images of templated Ti Petri dishes. The long-range hexagonal ordering and the vertical sidewalls of the resulting dishes can be clearly seen from these images. To confirm the resulting metal Petri dishes are composed of pure metals, we conducted wet etching experiments. After dipping the Au and Ti Petri dish samples in the corresponding metal etchants, all Petri dishes were gone in less than 1 min. The wall thickness of the templated Au and Ti Petri dishes is measured to be 53 ± 7 nm and 51 ± 5 nm, respectively, by averaging over 20 dishes. These thicknesses are very close to the thickness of the deposited metals (50 nm). This clearly indicates that the sputtering deposition is isotropic, and the wall thickness of the templated metal Petri dishes is determined by the sputtering thickness. The volume and the number density of metallic Petri dishes templated from 300 nm silica spheres are estimated to be ~10 attoliter/dish and ~$6 \times 10^8$ dishes/$cm^2$, respectively,

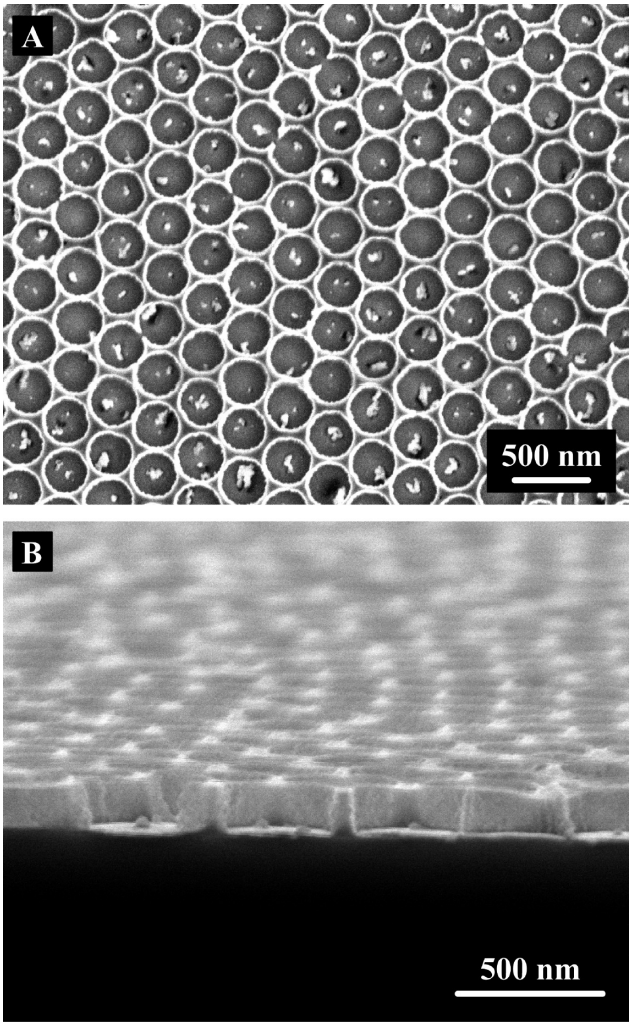


**Figure 7.** (A) Top and (B) side-view SEM images of the Au sample as shown in Figure 6C after lifting-off sacrificial Cr.

by a simple geometrical calculation. In Figure 8, it seems like the templated Ti Petri dishes are more densely packed than the Au dishes. Indeed the number density of the resulting Petri dishes is solely determined by the crystalline quality and interparticle distance of the original silica colloidal crystals. It is evident that the Ti dish array exhibits better packing quality than the Au array. In addition, the small size difference between the Ti dishes (337 ± 10 nm) and Au dishes (330 ± 11 nm) also contributes to the observed difference in packing density. The templated metallic Petri dishes can even be released from the silicon substrate to form stable dispersion by a brief hydrofluoric acid (2% aqueous solution) wash.

Metallic nanostructures with sharp features (e.g., nanocrescent moons, nanoprisms, nanopyramids, and nanorings) have been extensively exploited as surface-enhanced Raman scattering (SERS) substrates.[15,40,41] The sharp edges and tips can efficiently concentrate electromagnetic field, resulting in a great enhancement of Raman scattering intensity from molecules in the

(40) Aizpurua, J.; Hanarp, P.; Sutherland, D. S.; Kall, M.; Bryant, G. W.; de Abajo, F. J. G. *Phys. Rev. Lett.* **2003**, *90*, 057401.
(41) Jin, R. C.; Cao, Y. C.; Hao, E. C.; Metraux, G. S.; Schatz, G. C.; Mirkin, C. A. *Nature* **2003**, *425*, 487.

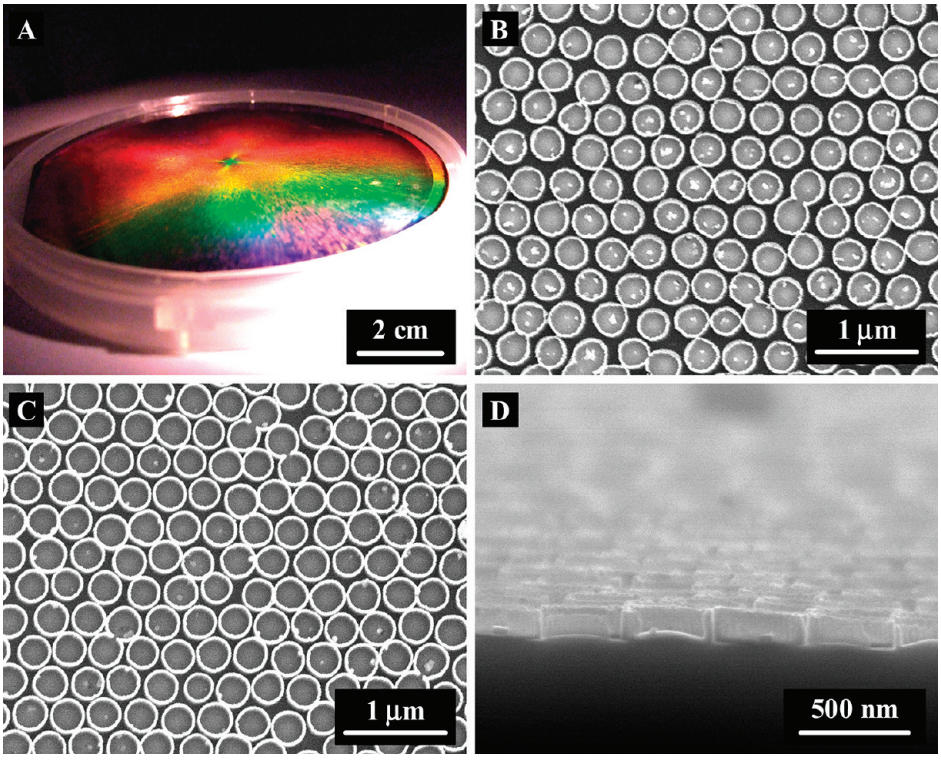


**Figure 8.** (A) Photograph of templated Au Petri dishes on a 4-in.-diameter silicon wafer. (B) Top-view SEM image of the same sample as in (A). (C) Top-view SEM image of Ti Petri dishes. (D) Side-view SEM image of the same sample as in (C).

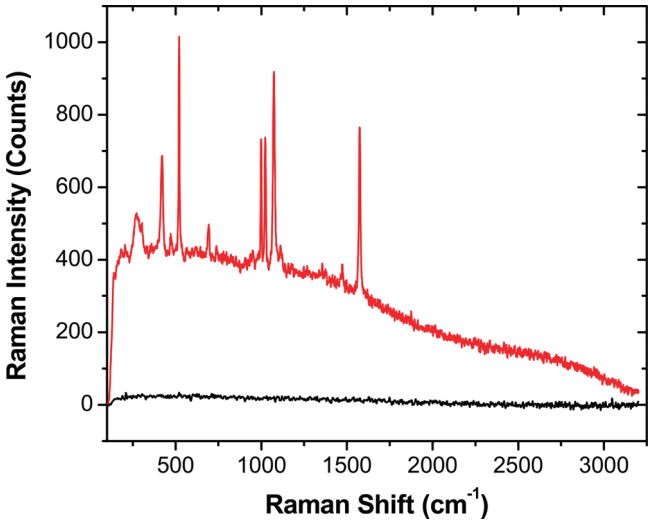


**Figure 9.** SER spectra of benzenethiol molecules adsorbed on a periodic array of Au Petri dishes templated from 300 nm silica spheres (red line) and a flat gold control sample (black line).

vicinity of these electromagnetic "hot spots".[15,31] The templated metallic Petri dishes have sharp edges, and the sharpness can be easily tuned by adjusting the thickness of the sputtered metal. We evaluate the SERS performance of periodic arrays of Au Petri dishes by using benzenethiol as a model molecule due to its large Raman cross-section and its ability to assemble into dense monolayers on Au.[11] Figure 9 compares the SER spectra of benzenethiol molecules adsorbed on Au Petri dishes with 50 nm thick sidewalls and a flat Au control sample prepared by the same sputtering process. Similar surface roughness of the Au control sample and the Au Petri dishes will facilitate to evaluate the contribution of the SERS enhancement from the roughness effect. The Au Petri dish arrays exhibit strong and distinctive SERS peaks whose positions and relative amplitude match with those in the literature for benzenethiol molecules adsorbed on structured gold surfaces;[42,43] while the featureless control sample shows no SERS signal. The SERS enhancement factor is calculated to be $9.1 \times 10^5$ and $9.3 \times 10^5$ using the method described in the literature by comparing the Raman intensity (after baseline correction) for two peaks at 1080 and 1581 $cm^{-1}$, respectively.[44] Although the templated Petri dishes have not been optimized for greatest SERS enhancement, they have shown higher enhancement factor than templated nanopyramids with nanoscale sharp tips.[31] Another significant advantage the templated Petri dishes offer over the previously reported nanoarrays (e.g., nanopyramids) in the context of SERS application is that the separation between neighboring EM "hot spots" (i.e., sharp edges) can be controlled in the nanoscale precision by tuning the thickness of the dielectric material sandwiched between two metal layers (e.g., Au-$SiO_2$−Au composite dishes). Previous studies show that the distance between EM "hot spots" plays a crucial role in determining the final SERS enhancement.[5,6] A systematic investigation on the structural parameters of metallic Petri dishes (e.g., size, separation, metal type, sidewall thickness, and even composite

(42) Cintra, S.; Abdelsalam, M. E.; Bartlett, P. N.; Baumberg, J. J.; Kelf, T. A.; Sugawara, Y.; Russell, A. E. *Faraday Discuss.* **2006**, *132*, 191.
(43) Abdelsalam, M. E.; Mahajan, S.; Bartlett, P. N.; Baumberg, J. J.; Russell, A. E. *J. Am. Chem. Soc.* **2007**, *129*, 7399.
(44) Tian, Z. Q.; Ren, B.; Wu, D. Y. *J. Phys. Chem. B* **2002**, *106*, 9463.

metal multilayers), which can greatly affect the localized surface-plasmon resonances and the resulting SERS enhancement, is under way.

## Conclusions

In conclusion, we have developed a novel templating approach for fabricating wafer-sized, periodic arrays of metallic Petri dishes with attoliter-scale volume. The size of the templated Petri dishes can be easily controlled by changing the diameter of the templating silica microspheres (70−1500 nm)[28,38] and the undercut amount of the polymer wetting layer. The depth of the Petri dishes is determined by the thickness of the polymer wetting layer. The thickness of the resulting Petri dishes can be adjusted by controlling the thickness of the sputtered metal. Composite Petri dishes consisting of multiple metals can also be fabricated by sequential sputtering deposition. Besides metallic Petri dishes, the current templating technology can be easily extended to a variety of other materials (e.g., ceramics), provided that these materials can be deposited by sputtering and they remain intact during the template removal processes. Our preliminary results also show that the templated Petri dishes can be loaded with other materials (e.g., KCl crystals) by controlled drying, promising for the miniaturization of analytical and bioanalytical techniques using these attoliter-scale nanocontainers. This bottom-up technology is scalable and compatible with standard microfabrication and could enable mass-production of periodic metallic nanostructures for applications ranging from biosensing to surface plasmon devices.

**Acknowledgment.** This work was supported in part by the NSF under Grant Nos. CBET-0651780 and CBET-0744879, the Defense Threat Reduction Agency, the start-up funds from the University of Florida, and the UF Research Opportunity Incentive Seed Fund. X. F. Liu acknowledges the China Scholarship Council for financial support.